Journal of Energy Chemistry 25 (2016) 985–993

Contents lists available at ScienceDirect

Journal of Energy Chemistry

journal homepage: www.elsevier.com/locate/jechem

http://www.journals.elsevier.com/journal-of-energy-chemistry/

Systematic variation of the sodium/sulfur promoter content on carbon-supported iron catalysts for the Fischer–Tropsch to olefins reaction☆

Martin Oschatz*, Nynke Krans, Jingxiu Xie, Krijn P. de Jong*

University of Utrecht, Group of Inorganic Chemistry and Catalysis, Universiteitsweg 99, 3584 CG Utrecht, The Netherlands

ARTICLE INFO

Article history:
Received 29 July 2016
Revised 22 September 2016
Accepted 16 October 2016
Available online 9 November 2016

Keywords:
Fischer–Tropsch to olefins synthesis
C_2–C_4 olefins
Iron catalysts
Promoters
Carbon supports

ABSTRACT

The Fischer–Tropsch to olefins (FTO) process is a method for the direct conversion of synthesis gas to lower C_2–C_4 olefins. Carbon-supported iron carbide nanoparticles are attractive catalysts for this reaction. The catalytic activity can be improved and undesired formation of alkanes can be suppressed by the addition of sodium and sulfur as promoters but the influence of their content and ratio remains poorly understood and the promoted catalysts often suffer from rapid deactivation due to particle growth. A series of carbon black-supported iron catalysts with similar iron content and nominal sodium/sulfur loadings of 1–30/0.5–5 wt% with respect to iron are prepared and characterized under FTO conditions at 1 and 10 bar syngas pressure to illuminate the influence of the promoter level on the catalytic properties. Iron particles and promoters undergo significant reorganization during FTO operation under industrially relevant conditions. Low sodium content (1–3 wt%) leads to a delay in iron carbide formation. Sodium contents of 15–30 wt% lead to rapid loss of catalytic activity due to the covering of the iron surface with promoters during particle growth under FTO operation. Higher activity and slower loss of activity are observed at low promoter contents (1–3 wt% sodium and 0.5–1 wt% sulfur) but a minimum amount of alkali is required to effectively suppress methane and C_2–C_4 paraffin formation. A reference catalyst support (carbide-derived carbon aerogel) shows that the optimum promoter level depends on iron particle size and support pore structure.

1. Introduction

Lower olefins (C_2–C_4) are crucial components for the production of plastics, solvents, coatings, or synthetic textiles [1]. Traditionally, these molecules are produced by steam cracking of naphtha or fluid catalytic cracking of vacuum gas oil [2]. In recent years, production routes based on alternative feedstocks reached considerable attention. Especially synthesis gas (a mixture of H_2 and CO) is attractive for lower olefins production because it can be produced from coal, natural gas, or biomass. Syngas can be converted to C_2–C_4 olefins by indirect routes via dimethyl ether or methanol intermediates [3,4]. Direct methods for their production from H_2/CO mixtures involve bifunctional catalysts [5,6] or the so-called Fischer–Tropsch to olefins (FTO) process with iron-based catalysts [7–9].

In FTO, iron(carbide)-based catalysts induce the dissociation of the reactants followed by the formation of CH_x species which associate and form hydrocarbons via chain growth [1,10]. Chain termination can occur either via hydrogenation or β-hydride abstraction, leading to the formation of alkanes or alkenes, respectively. Besides sufficient activity, minimum selectivity toward low-value methane and C_2–C_4 paraffins as well as stable operation under industrially relevant conditions are the most important requirements for iron-based FTO catalysts. The iron nanoparticles are often dispersed over nanostructured inorganic support materials to avoid excessive growth and mechanical breakdown [11]. Because iron carbide is the catalytically active phase, weakly interactive carbon supports lead to higher catalytic activity as compared to strongly interacting high surface area oxides due to the likely formation of hardly reducible iron species in the latter during catalyst calcination [12]. Numerous approaches for the synthesis of iron-based FTO catalysts on carbon supports have been reported [9,13–17]. The size of the iron particles, the strength of their encapsulation into the support, and the textural properties of the supports are crucial factors for the properties of the catalysts as well [18–22]. Functionalization of the support surface [23–25] as well as the addition

☆ This work was supported by a PostDoc grant of the German Academic Exchange Service (Deutscher Akademischer Austauschdienst, DAAD grant no. 91552012) and by the European Research Council (EU FP7 ERC advanced grant no. 338846).

* Corresponding authors.
E-mail addresses: M.Oschatz@uu.nl (M. Oschatz), K.P.deJong@uu.nl (K.P. de Jong).

http://dx.doi.org/10.1016/j.jechem.2016.10.011

of promoters [7,26,27] can suppress the formation of methane and increase selectivity toward lower olefins as well as the catalytic activity. Especially a combination of sodium and sulfur as the promoters enhances the catalytic properties. Particle size investigations as well as theoretical studies have been carried out to illuminate their binding state on the iron carbide particles and effects on product formation in the FTO process [18,28,29]. Sulfur can restrict the termination of carbon chain growth through hydrogenation thus favoring the β-hydride abstraction pathway. However, such promoted catalysts suffer from rapid deactivation due to particle growth, especially under industrially relevant conditions [18]. It is generally known that iron and the promoters can undergo significant structural changes and reorganization during catalyst operation [30].

Although the overall advantage of the use of combined sodium/sulfur promoters has been shown in multiple studies [18,28,29,31], no systematic variation of their ratio was carried out for carbon-supported iron catalysts. Zhou et al. and Xu et al. varied the sulfur content for α-Al_2O_3-supported iron catalysts but at constant sodium content or without alkali [32,33]. Torres Galvis et al. showed the effect of a promoter ratio variation for Fe/α-Al_2O_3 catalysts but no systematic investigation was carried out [29]. For carbon supports, no systematic study over a sufficiently wide range of promoter levels was reported so far at constant iron loading. Recently, it could be shown for iron on ordered mesoporous carbon supports, that the additional presence of sulfur on sodium-promoted iron-based catalyst increases the catalytic activity and suppresses methane formation but no optimization of the promoter ratio was carried out. Within the investigated range of sulfur contents, the catalytic activities and selectivities showed no significant changes [34].

In this study, we systematically investigate the interplay between the ratio of sodium and sulfur promoters for iron particles of comparable size and loading on a carbon black support. Nominal loadings of 1–30 wt% sodium and 0.5–5 wt% sulfur with respect to iron are applied. All catalysts show significant initial catalytic activity after iron carbide formation. The latter is accelerated at higher sodium loadings. Catalyst deactivation occurs mainly by particle growth leading to a lowering of the catalytically active surface area. In the presence of large amounts of sodium and sulfur this leads to a complete loss of activity, likely due to covering of the active sites with promoters. Low sodium loadings cause higher initial activity after carbide formation and higher activity can be maintained over time on stream. However, a minimum amount of sodium seems needed to ensure efficient suppression of hydrogenation by sulfur. Finally, we show that a similar promoter ratio leads to significant differences depending on the iron particle size and the support pore structure.

2. Experimental

2.1. Catalyst synthesis

Iron-based FTO catalysts were prepared by the incipient wetness impregnation (IWI) technique. Porous carbon black (CB) with a specific surface area of 1100 m^2/g was used as the support material. 270 mg of the carbon was impregnated in a mortar with 1 ml of an aqueous solution of 187.5 mg ammonium iron(III)citrate (Fluka, 14.5–16 wt% iron) to achieve a nominal iron loading of ~10 wt%. For the catalysts with sodium/sulfur promoters, sodium citrate dihydrate (99%, Sigma Aldrich) and iron(II)sulfate heptahydrate (99%, Sigma Aldrich) were added to the impregnation solution. Sodium loadings of 30, 15, 3, and 1 wt% were targeted with respect to iron and nominal sulfur loadings were 5, 3, 1, and 0.5 wt% with respect to iron. After impregnation, the catalysts were dried overnight at 120 °C under static air. Calcination was carried out at 500 °C (heating rate 2 °C/min) for 2 h in a glass tube in a tubular furnace under nitrogen flow. Catalysts are labeled according to their theoretical sodium and sulfur ratios (in wt%-with respect to iron). For example, the catalysts with a theoretical sodium content of 30 wt% and a theoretical sulfur content of 5% with respect to iron is labeled as "Fe/CB–Na_{30}–S_5". The catalyst without extra addition of sodium and sulfur is labeled "Fe/CB-unpromoted". The synthesis of the carbide-derived carbon (CDC) aerogel support material used for the reference catalyst was carried out at 700 °C as described elsewhere [35]. The as-obtained CDC underwent a post-synthesis oxidation treatment under air atmosphere at 400 °C for 1 h in a muffle furnace to enhance the wetting of the highly hydrophobic CDC surface with the aqueous impregnation solution. Otherwise, the synthesis of the Fe/CDCAero–Na_3–S_1 catalyst was carried out similar to the Fe/CB–Na_3–S_1. ICP-OES analysis of the reference catalyst shows a content of 7.8 wt% iron, 0.3 wt% sodium, and 0.09 wt% sulfur.

2.2. Catalyst characterization

Iron, sodium, and sulfur contents of the calcined catalysts were determined with inductively coupled plasma-optical emission spectroscopy (ICP-OES). The measurements were performed with a SPECTRO ARCOS ICP-OES instrument after aqua regia extraction of the samples.

Nitrogen physisorption isotherms were measured at −196 °C at a Micromeritics TriStar 3000 apparatus. The specific surface area of the support was calculated with the multi-point BET equation ($0.05 < p/p_0 < 0.25$). The total pore volume was determined at $p/p_0 = 0.995$. The t-plot method was used for the determination of the micropore surface area.

Transmission electron microscopy (TEM) and high angle annular dark field (HAADF) scanning transmission electron microscopy (STEM) measurements were performed using an FEI Tecnai 20 FEG instrument, operating at 200 kV. Prior to the measurements, the samples were ground into fine powders, dispersed in ethanol, sonicated for ~30 s, and drop-casted on a carbon-coated copper TEM grid.

2.3. Catalytic testing at 1 bar

Catalytic testing under Fischer–Tropsch conditions at 1 bar was performed at 350 °C, H_2/CO ratio of 1/1 by volume, and a GHSV of ~3600 h^{-1}. The FTO reaction was carried out at low conversions of CO (<1%) to minimize the extent of secondary reactions and heat transfer limitations. Calcined catalysts were sieved to a particle size fraction of 75–212 µm. 100 µL of catalyst were mixed with 100 µL silicon carbide (212–425 µm) and transferred to a plug flow fixed-bed reactor. Prior to Fischer–Tropsch reaction, catalysts were reduced in situ for 2 h at 350 °C (heating rate 5 °C/min) in 15 mL/min of a H_2/He mixture (1/2 by volume) followed by cooling to 290 °C. Then, the flow was changed to 6 mL/min of a H_2/CO mixture (1/1 by volume) to allow carbide formation under mild conditions for 1 h. For the FTO reaction, the temperature was increased to 350 °C again (time on stream; TOS = 0 h when temperature reached 350 °C). The C_1–C_{16} products were analyzed with an online gas chromatograph Varian CP3800 equipped with an FID detector. The product selectivity in $\%_{Carbon}$ was calculated as equivalent of carbon atoms present in a product fraction in relation to total carbon atoms present in the formed hydrocarbons. The CO_2 selectivity was not measured for the experiments at 1 bar. The activity of the catalysts is expressed as iron time yield (FTY) in moles of converted CO to hydrocarbons per gram of iron per second.

2.4. Catalytic testing at 10 bar

Testing of the FTO catalysts under industrially relevant conditions was performed in a 16 reactor catalytic testing setup (Flowrence, Avantium) at 10 bar, 340 °C, H_2/CO ratio of 2/1 by volume, and a GHSV of ~3600 h^{-1}. Calcined catalysts were sieved to a particle size fraction of 75–212 µm. ~20 mg of catalyst were diluted with 100 µL silicon carbide (212–425 µm) and transferred to a tubular fixed-bed reactor. The catalysts were dried in a He flow at 280 °C for 20 min at 3 bar followed by subsequent change to a flow of H_2/CO mixture (2/1 by volume) at 280 °C and 3 bar for 10 min. Then, the temperature was increased to 340 °C (heating rate 2 °C/min) and after 10 min, the pressure was increased to 10 bar (TOS = 0 h). The products were analyzed using online gas chromatography (Agilent 7890A). The permanent gases and CO_2 were separated on a ShinCarbon ST column and quantified against He as an internal standard using a TCD detector. CO conversions were calculated as $X_{CO} = (mol_{CO,in} - mol_{CO,out})/mol_{CO,in}$. Hydrocarbons ($C_1$–$C_9$) were separated on an Agilent J&W PoraBOND Q column, detected using an FID detector and quantified against the TCD signal of the internal standard He. As for the FTO measurements at 1 bar, product selectivity in the formed hydrocarbons was calculated based on a carbon atom basis. For FTO at 10 bar, with the exceptions of the Fe/CB–Na_1–S_1 (32%) and Fe/CB–Na_1–$S_{0.5}$ (47%), all selectivities are reported at CO conversions of 20%–30%. At the end of the catalytic testing experiment, the reactors were cooled down to room temperature under a flow of He.

3. Results and discussion

The used support material is a porous carbon black (CB) composed of agglomerated and branched carbon particles with near-spherical morphology. In addition to the pores originating from the inter-particular space, some hollow carbon particles can also be observed the TEM images (Fig. 1). The CB material provides a high specific surface area of 1100 m^2/g and the total pore volume (for pores < ~350 nm in diameter) is 2.34 cm^3/g. The step increase of the nitrogen physisorption isotherm (Fig. S1, Supporting Information) at relative pressures $p/p_0 > 0.9$ shows that the pore volume is mainly provided by a distinctive meso- and macropore system as it is typical for highly branched CBs with broad pore size distribution. T-plot analysis shows the presence of a small micropore specific surface area of 71 m^2/g in the CB support. Especially the sodium ions are expected to have particular affinity to adsorb in these narrow cavities. Since the same support material was used for all catalysts, the porosity will have the same influence on the distribution of iron and the promoters in all cases.

ICP-OES measurements of the calcined catalysts (Table 1) show that the IWI impregnation technique allows precise control over the compositions of the catalysts. The iron contents are in the same range for all catalysts but slightly below the targeted values of 10 wt% due to the ill-defined stoichiometry of the ammonium iron(III)citrate precursor and/or traces of water. The amount of sodium promoter in relation to iron is well controllable and in the same range for the catalysts with the same targeted amount of alkali. The trend in sulfur distribution within the catalyst series also matches the targeted tendencies. Despite the low over-all sulfur content and hence high uncertainty of the ICP-OES analysis, it should be noticed that the sulfur content of all promoted catalysts is slightly above the targeted loadings. Traces of sulfur and sodium were also detected in the catalyst Fe/CB-unpromoted, likely originating from the pristine CB support and/or the iron precursor salt. From the elemental compositions of the catalysts, it can be concluded that the catalyst synthesis with the IWI method followed by drying and calcination allows precise control over the catalyst composition. Differences in the catalytic properties will not result from inaccurate variations in the catalyst compositions in terms of iron loading and/or promoter levels, rendering this series of catalysts qualified to investigate the influence of different promoter levels on iron-based FTO catalysts.

Table 1. ICP-OES data of the calcined promoted FTO catalysts.

Catalyst	Fe (wt%)	Na (wt%)	S (wt%)
Fe/CB–Na_{30}–S_1	7.3	2.3	0.22
Fe/CB–Na_{30}–S_3	7.7	2.4	0.39
Fe/CB–Na_{30}–S_5	7.5	2.1	0.49
Fe/CB–Na_{15}–S_1	7.4	1.2	0.25
Fe/CB–Na_{15}–S_3	7.9	1.2	0.40
Fe/CB–Na_{15}–S_5	8.2	1.2	0.53
Fe/CB–Na_3–$S_{0.5}$	8.6	0.3	0.22
Fe/CB–Na_3–S_1	8.4	0.3	0.26
Fe/CB–Na_3–S_3	7.9	0.3	0.40
Fe/CB–Na_3–S_5	7.9	0.3	0.52
Fe/CB–Na_1–$S_{0.5}$	8.6	0.1	0.21
Fe/CB–Na_1–S_1	8.4	0.2	0.23
Fe/CB-unpromoted	9.5	0.1	0.20

Previous studies have shown that the size of the metal particles has significant influence on the catalytic properties of iron-based FTO catalysts [19]. TEM investigations of calcined catalysts with high (Fe/CB–Na_{30}–S_5) and low (Fe/CB–Na_3–S_1) promoter level and without promoters (Fe/CB-unpromoted) show the presence of well-dispersed iron particles over the surface of the carbon support (Fig. 1). No larger agglomerates or iron particles can be observed. The average size of the iron particles was determined to be 5.6 ± 1.4 nm in the Fe/CB-unpromoted catalyst after calcination. The promoted catalysts investigated exhibit slightly lower particle sizes of 4.7 ± 1.0 nm (Fe/CB–Na_3–S_1) and 4.2 ± 1.0 nm (Fe/CB–Na_{30}–S_5) (Fig. S2). Since these catalysts have different promoter content and show comparable iron particle sizes, it can be expected that the initial particle sizes will only have a minor influence on the differences in the catalytic properties of the catalysts with similar metal loading on the same support. It is noted that these initial particle sizes are above the range where significant particle size effects are apparent [18,19].

Selected CB-supported catalysts were first tested under FTO conditions at 1 bar, 350 °C, H_2/CO = 1, and a GHSV of 3600 h^{-1} (Fig. S3 and Table S1). Stable catalytic activity is achieved after activation at 350 °C under diluted hydrogen, followed by carburization of the iron at 290 °C under syngas. Previously reported iron-based FTO catalysts with ordered mesoporous CMK-3 carbon as the support showed constant increase of the catalytic activity after the first hours of time on stream after comparable activation treatments [34]. Carbide formation seems to be enhanced in case of the CB support, facilitating the reactivity of the iron species with syngas. No significant decrease of the catalytic activity is observed within the first 18 h of time on stream (TOS) (Fig. S3). However, due to the low CO conversions (and hence relatively high experimental error) and the generally higher stability under FTO conditions at 1 bar, the influence of the promoter levels on the activities and stabilities of the different catalysts will be discussed in detail for the FTO experiments at 10 bar.

In contrast, the influence of sodium and sulfur on the product selectivity can be investigated in a straightforward way at 1 bar because heat transfer limitations within the reactor and secondary reactions between FTO products are minimized at low CO conversions. All promoted catalysts show a higher formation of C_2–C_4 olefins (up to 67%$_C$ of the formed hydrocarbons), lower methane selectivity (8–14%$_C$), and higher chain growth probability (α = 0.57–0.80) as compared to the catalyst without additional loading of sodium and sulfur (Table S1). In agreement with previous studies, the higher olefin/paraffin ratio in the C_2–C_4 area as well as the lower methane selectivity of the promoted catalysts is resulting from the addition of sulfur, leading to preferred chain ter-

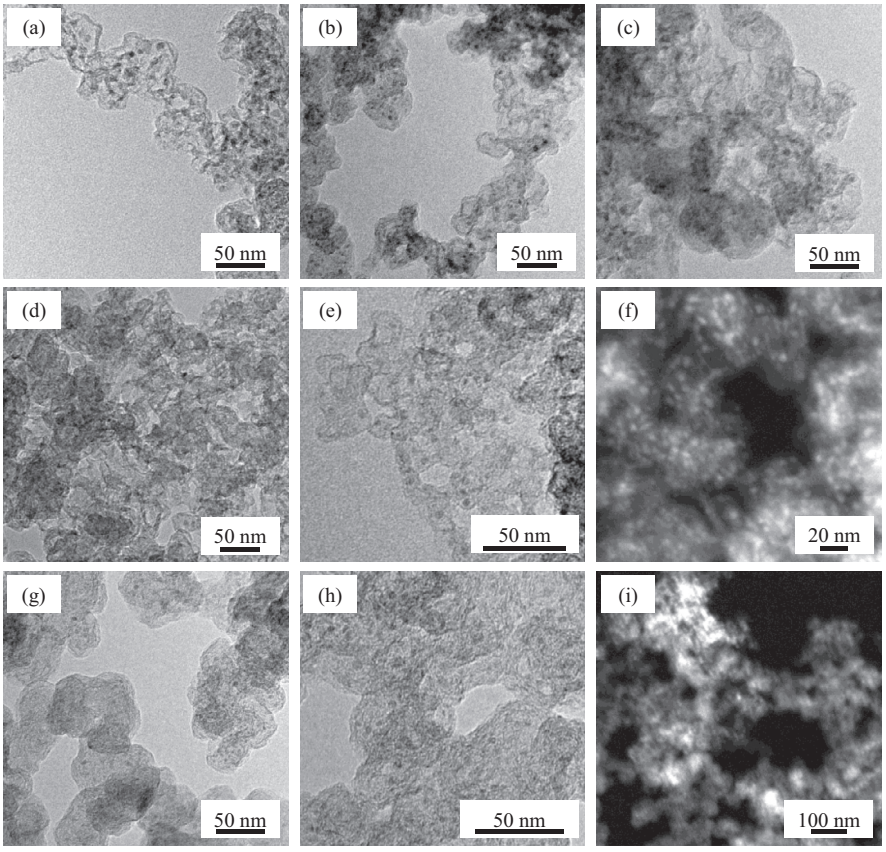

Fig. 1. TEM and HAADF-TEM images of the Fe/CB-unpromoted catalyst (a–c) and the promoted Fe/CB–Na_{30}–S_5 (d–f) and Fe/CB–Na_3–S_1 (g–i) catalysts.

mination by β-hydride abstraction by blocking hydrogenation sides of the catalysts [28,29]. In tendency, α decreases with decreasing sodium content for catalysts with similar sulfur loading and the C_{5+} product fraction is smaller for the catalysts with low sodium content. Although no significant effect of the sulfur promoter on the chain growth probability and the C_2–C_4 olefin formation is observed in the range of investigated loadings, it can be seen that the catalysts with the lower sulfur contents tend to have higher methane selectivities and lower olefin/paraffin ratios in the C_2–C_4 range. This supports the hypothesis that sulfur blocks the hydrogenation sides of the iron particles. However, for CB-supported iron particles of the investigated size, further increase of the sulfur content to 3 or 5 wt% related to iron leads to only moderate decrease of methane and C_2–C_4 paraffin formation.

While catalytic testing at 1 bar and low CO conversion is most suitable for the profound investigation of the selectivity, the catalysts were also tested at 10 bar syngas pressure, 340 °C, and $H_2/CO = 2$, to investigate their properties at higher maximum CO conversions between 27% and 76% (Fig. 2, Table S2, and Fig. S4). In terms of activity and stability, it can be seen that the Fe/CB-unpromoted catalyst increases in activity during the first 40 h TOS and then operates at nearly constant CO conversion with very slow deactivation (Fig. 2b). Our group recently studied a series of promoted and unpromoted carbon fiber-supported FTO catalysts and it was shown that iron carbide formation is slow in absence of promoters [18], leading to ongoing activation of the catalysts during high-pressure FTO operation. Also in agreement with this study, all promoted catalysts decrease in activity in the first 100 h of TOS. Interestingly, the catalysts with low sodium content of 3 and 1 wt% related to iron show a longer "induction period" during the first hours of FTO operation which is not required at higher sodium contents (Fig. 3a, b and Fig. S4A, B). Sodium hence accelerates the formation of iron carbide species in agreement with previous findings. For catalysts with similar sodium content, the duration of this activation period increases with increasing sulfur content. Although sodium facilitates iron carbide formation, catalysts with lower promoter content provide higher initial catalytic activity after the induction period (Fig. 3a, b). Sodium and sulfur can block catalytically active sites of the iron carbide particles and thus reduce the activity. After reaching a maximum, the activity of all catalysts decreases. However, the decrease is significantly slower at low sodium contents. For similar sodium content, the loss of activity is slower for the catalysts with low sulfur content. With the exception of the Fe/CB–Na_3–S_3 catalyst, the CO conversion of all samples with sulfur contents of 3 and 5 wt% go down close to zero within the first 40 h of TOS. Considering this rapid deactivation, the iron particles with this particular support and metal content be considered as being "overpromoted" with sulfur because an increase of the sulfur content leads to more rapid decrease in activity but does not lead to enhancement of the catalyst selectivity.

Comparable to the experiments under FTO conditions at 1 bar, the differences in the selectivities for catalysts with sodium contents of 15 and 30 wt% remain low. At CO conversions of 20%–30%, all catalysts show methane selectivities of ~12%$_C$, C_2–C_4 olefin selectivities of ~58%$_C$, and C_{5+} selectivities of ~24%$_C$ (Table S2). All catalysts deviate from the Anderson–Schulz–Flory (ASF) distribution in terms of C_1 and C_2 production (Fig. S4C, D) and show comparable chain growth probability ($\alpha = 0.54$–0.56) (Table S2).

Further lowering of the sodium content to 3–1 wt% related to iron has more distinct effect on the selectivity values (Fig. 2c, d and Table S2). The Fe/CB–Na_3–S_1 catalyst still exhibits comparable C_2–C_4 olefins selectivity (57.6%$_C$) as compared to the catalysts with higher promoter content. Similar as at 1 bar, the C_2–C_4 paraffin selectivity (7.9%$_C$) and the methane selectivity (14.4%$_C$) increase

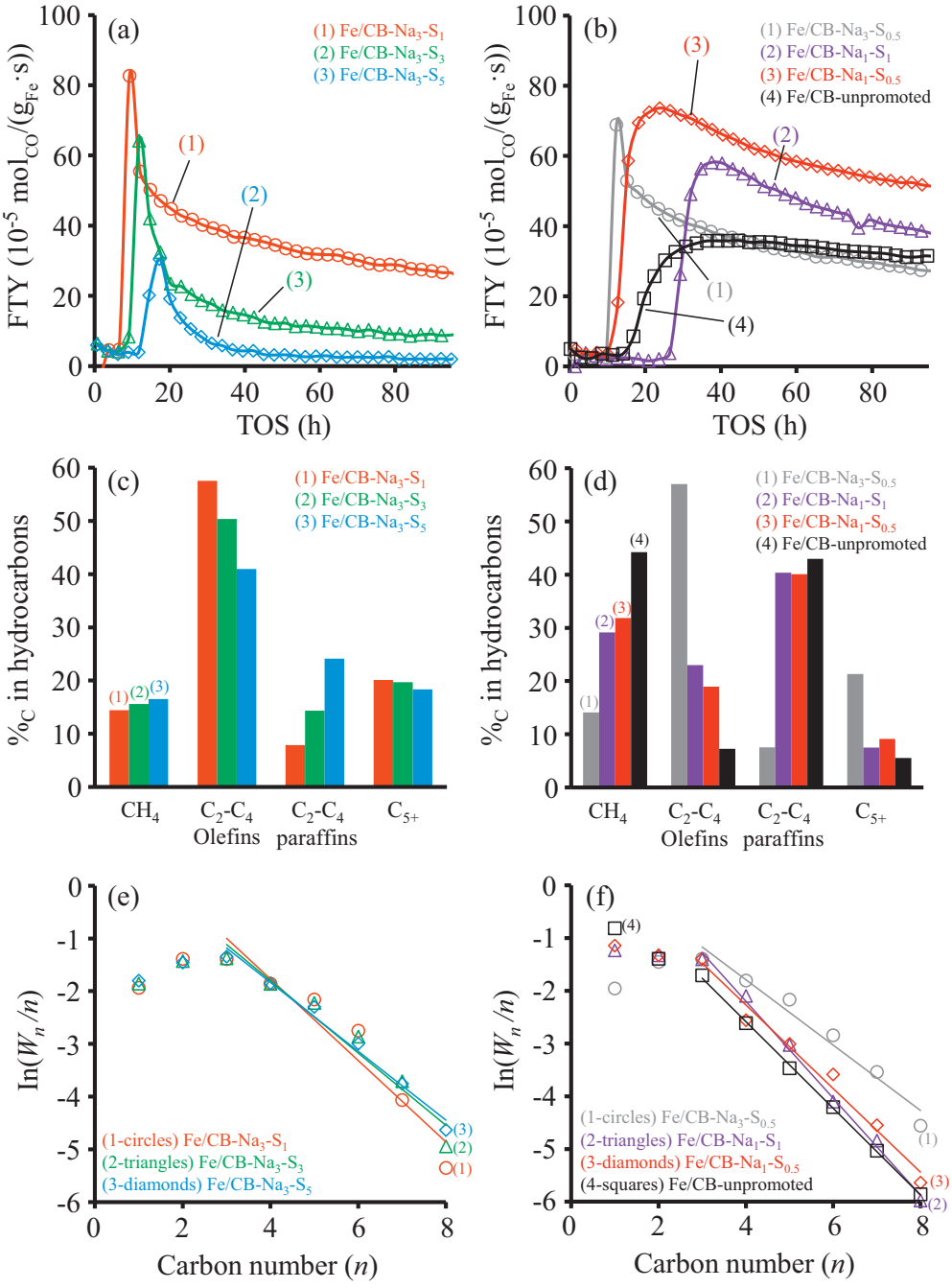

Fig. 2. Iron-weight based activity (FTY) over TOS (a, b), product selectivity based on the formed hydrocarbons (c, d), and corresponding Anderson–Schulz–Flory (ASF) plots of the C_1–C_8 product fractions with chain growth probability (α) based on the C_3–C_8 products (e, f) of the Fe/CB catalysts with sodium contents of 1 and 3 wt% and the Fe/CB-unpromoted catalyst under industrially relevant FTO conditions at 10 bar.

whereas the C_{5+} selectivity (20.1%$_C$) and the chain growth probability ($\alpha = 0.46$) decrease with decreasing sodium content at similar sulfur loading. With the exception of α, the same changes are observed if the sulfur loading is increased to 3 or 5 wt% at a constant sodium content of 3 wt%. Lowering of the sulfur content to 0.5 wt% has neither large effect on catalytic activity, nor on the selectivity. Only an increase of the chain growth probability to $\alpha = 0.54$ occurs. In contrast, lowering of the sodium content to 1 wt% leads to a significant increase of the methane and C_2–C_4 paraffin formation and decrease of lower olefins and C_{5+} selectivity for the Fe/CB–Na_1–S_1 catalyst (Fig. 2d). The same effect occurs if both sodium and sulfur ratios are lowered to 1 and 0.5 wt%, respectively. However, although the enhancement of the selectivity at low concentrations of sodium and sulfur gets smaller and although the elemental compositions determined by ICP-OES are comparable, the Fe/CB–Na_1–S_1 and Fe/CB–Na_1–$S_{0.5}$ still show lower methane formation, higher C_2–C_4 olefins selectivity, and higher C_{5+} formation as compared to catalyst Fe/CB-unpromoted.

For this series of catalysts it can be concluded that the activity of the catalysts increases at lower amount of sodium and sulfur due to the higher number of available catalytically active sites as compared to catalysts with higher promoter levels and enhanced carbidization as compared to the Fe/CB-unpromoted catalyst. Furthermore, there is a certain amount of sodium required to sup-

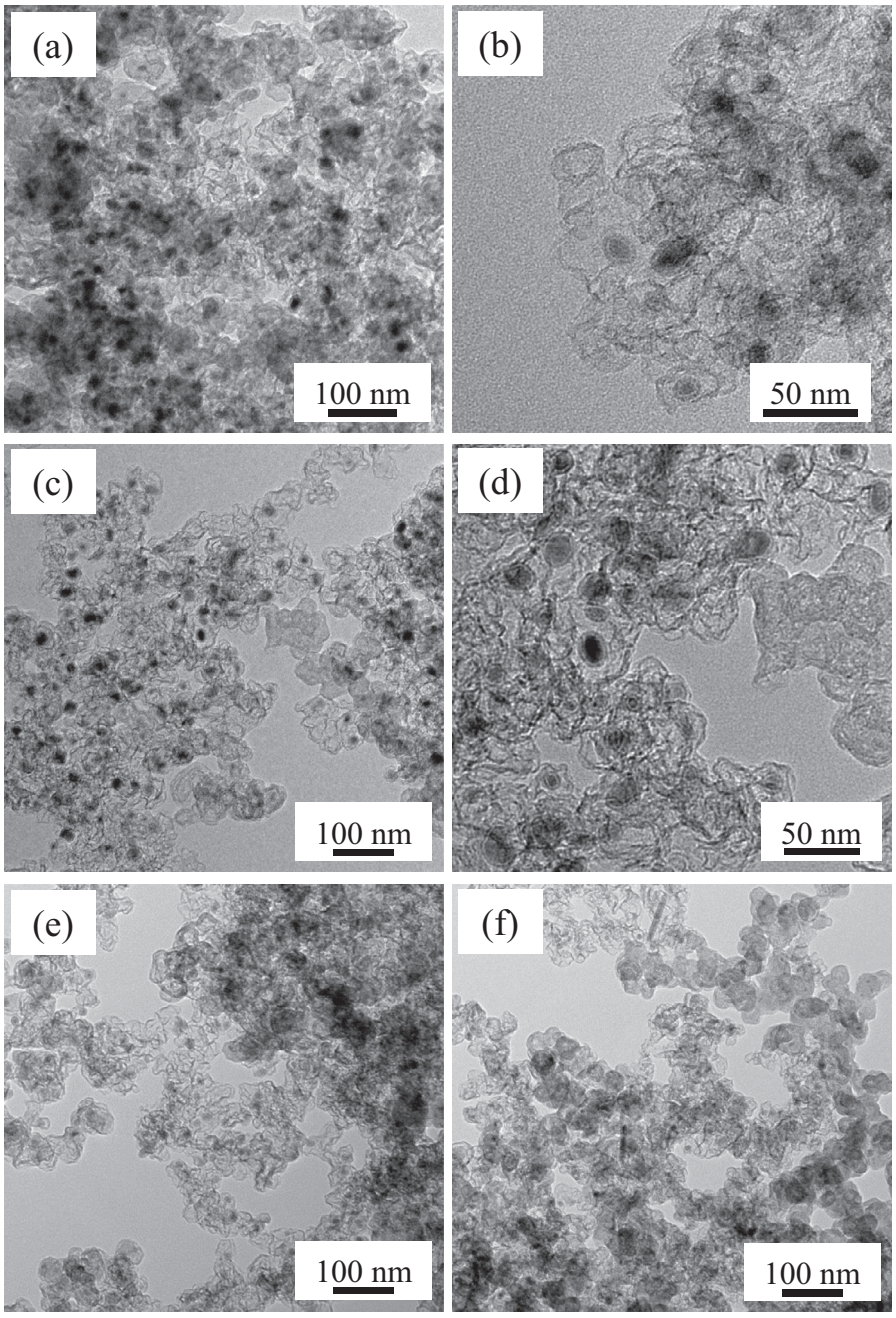

Fig. 3. TEM images of the spent catalysts Fe/CB–Na_3–S_1 (a, b), Fe/CB–Na_{30}–S_5 (c, d), and Fe/CB-unpromoted (e, f) after ~140 h of TOS under industrially relevant FTO conditions at 10 bar.

press the formation of methane by sulfur addition. For the applied carbon black support and iron loading, optimum promoter levels are present on the Fe/CB–Na_3–$S_{0.5}$ and Fe/CB–Na_3–S_1 catalysts because they combine high initial catalytic activity after the activation period and slower deactivation as compared to the catalysts with higher sodium and/or sulfur contents. At the same time, they show higher selectivity to lower olefins and suppressed methane formation in comparison to the catalysts with lower alkali content. The catalysts with 3 wt% sodium significantly deviate from the ASF product distributions in the C_1 and C_2 range independent of the sulfur ratio. In contrast, the catalysts with 1% sodium show a ASF distribution which is comparable to the Fe/CB-unpromoted catalyst (Fig. 2e, f). In a recent study on sodium/sulfur promoted iron-based FTO catalysts on carbon supports it was shown that sodium (alone in combination with oxygen) cannot suppress methane formation significantly below the ASF predictions [34]. Sodium plus sulfur seems necessary to suppress methane formation but apparently needs a certain concentration for effective operation.

The CO_2 selectivity of all promoted catalysts is in the range of 40–45%$_C$. It does not change significantly or follows a trend with changing promoter concentration but decreases to 35%$_C$ without extra addition of promoters. This indicates that this promoter combination does not only change the activity and product selectivity of the CO hydrogenation process but also influences the water-gas-shift activity of the iron catalysts.

The most likely reason for deactivation of the catalysts during FTO operation is particle growth (Fig. 3). The average particle size of the spent Fe/CB–Na_3–S_1 and Fe/CB–Na_{30}–S_5 catalysts increases

to 16 ± 5 nm and 18 ± 4 nm, respectively after 140 h of TOS under industrially relevant FTO conditions (Fig. S5). The iron particles are significantly larger in size as compared to the calcined catalysts and show a typical shape and core-shell structure due to the formation of an iron oxide passivation layer on the iron carbide surface after exposure of the spent catalysts to air. Although the iron particle sizes in both spent catalysts are comparable, the sample with the lower promoter level still showed significant iron time yield after FTO operation whereas the catalyst with high promoter level shows no catalytic activity anymore after only ~40 h of TOS. A likely reason is the complete coverage of catalytically active iron carbide surface with sodium and sulfur in the Fe/CB–Na_{30}–S_5. During particle growth, the available surface area decreases and hence an increasing coverage with promoters can occur. Although the available iron surface of both spent catalysts is comparable due to comparable particle sizes, the increasing coverage of the particles with promoters during particle growth leads to a complete loss of the catalytic activity of the Fe/CB–Na_{30}–S_5. In contrast, Fe/CB–Na_3–S_1 still shows significant activity at similar iron particle size. After ~100 h TOS, the GHSV was decreased from ~3600 to ~1800 h^{-1} and the CO conversion increases for the Fe/CB–Na_3–S_1 at nearly unchanged FTY whereas the Fe/CB–Na_{30}–S_5 shows no response to the lower gas flow due to the complete blocking of the catalytically active surface (Fig. S6).

The Fe/CB–Na_1–S_1 and Fe/CB–Na_1–$S_{0.5}$ catalysts show higher initial activity but comparable deactivation behavior as compared to Fe/CB–Na_3–S_1 (Fig. 2a, b). This suggests that particle growth is the main reason for the decreasing activity in these catalysts as well and their activity remains higher over TOS due to the lower promoter concentration on the iron surface. However, a generally slower growth of the particles leading to slower catalyst deactivation at lower promoter concentrations cannot be ruled out. In agreement with a previous study on carbon nanofiber-supported FTO catalysts, the Fe/CB-unpromoted catalyst shows a lower average iron particle size of 11 ± 3 nm as compared to the promoted catalysts after 140 h of TOS under industrially relevant FTO conditions (Fig. 3e, f and Fig. S5).

After the carbide formation in the initial activation period, the selectivity of the Fe/CB–Na_3–S_1 catalyst changes with iron particle size and promoter distribution. At the high initial CO conversion, a larger iron particle surface area is available and the low promoter content leads to higher C_2–C_4 paraffin formation which then decreases over time (Fig. 4a). In contrast, the C_2–C_4 olefins selectivity increases with TOS due to proceeding particle growth associated with the decrease of the number of corners and edges and higher surface concentration of the promoters. Under FTO conditions at 1 bar, the catalysts show more stable activity because less particle growth occurs at low CO conversion (Fig. 4b) [34]. Accordingly, after the first 2–4 h of TOS, stable selectivity is observed due to rather constant iron particle size and promoter concentration on their surface.

The influences of the promoter levels on activity, selectivity, and stability of the iron-based FTO catalysts will vary significantly with iron particle size and support pore structure. As a reference catalyst, we introduce a Fe/CDCAero–Na_3–S_1 with a nominal elemental composition similar to Fe/CB–Na_3–S_1. It should be noticed that the sulfur content of this catalyst (estimated with ICP-OES) is slightly lower as compared to the carbon black-supported analogue, likely due to the presence of traces of sulfur in the pristine CB. The carbide-derived carbon (CDC) aerogel support also consists of agglomerated carbon nanoparticles with high inter-particular porosity (Fig. 5a, b). In contrast to the carbon black, this material provides a much larger micropore surface area of ~1034 m^2/g (Fig. S1). This leads to different distribution of iron and the promoters over the support. Some iron particles in the same size range as for the CB support can be observed in the TEM images after calcination but the different pore structure of the CDC aerogels can also lead to the presence of smaller particles in the micropores of the CDC. Under industrially relevant FTO conditions, the CDC aerogel-supported catalyst also shows the typical induction period and FTY comparable to the Fe/CB–Na_3–S_1 catalyst. However, slower loss of catalytic activity is observed over time on stream for the Fe/CDCAero–Na_3–S_1 (Fig. 5c). This is likely caused by the distribution of promoters over the high support surface area and therefore lower blockage of iron carbide particle surface and by slower growth of iron particles with lower promoter concentration on the surface. The higher surface area of the CDC aerogel support might also provide a stronger physical binding of the iron carbide particles, leading to slower deactivation. Similar as for the CB-supported catalysts with lower promoter level, the Fe/CDCAero–Na_3–S_1 shows higher formation of C_2–C_4 paraffins instead of olefins as compared to the Fe/CB–Na_3–S_1 (Fig. 5d). The relatively high C_{5+} selectivity of the CDC aerogel-supported catalyst is likely caused by the higher CO conversion facilitating secondary reactions between the products. This comparison of two different support structures shows that the effect of promoter content is strongly influenced by the iron particle size and the support pore structure.

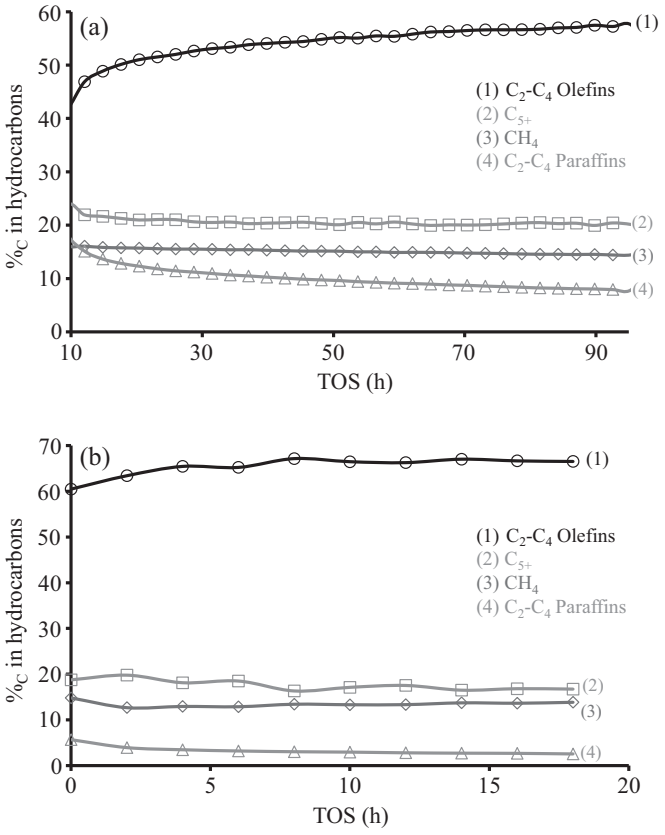

Fig. 4. Product selectivity distributions of the Fe/CB–Na_3–S_1 catalyst over TOS under FTO conditions at 10 bar (a) and 1 bar (b).

4. Conclusions

The influence of sodium/sulfur promoter levels on the properties of carbon black-supported iron-based Fischer–Tropsch to olefins catalysts was investigated by systematic variation of the nominal promoter loading between 1 and 30 wt% sodium and 0.5 and 5 wt% sulfur related to iron. Selectivity investigations under FTO conditions at 1 bar show that the chain growth probability and the C_{5+} selectivity decrease at lower sodium content and that

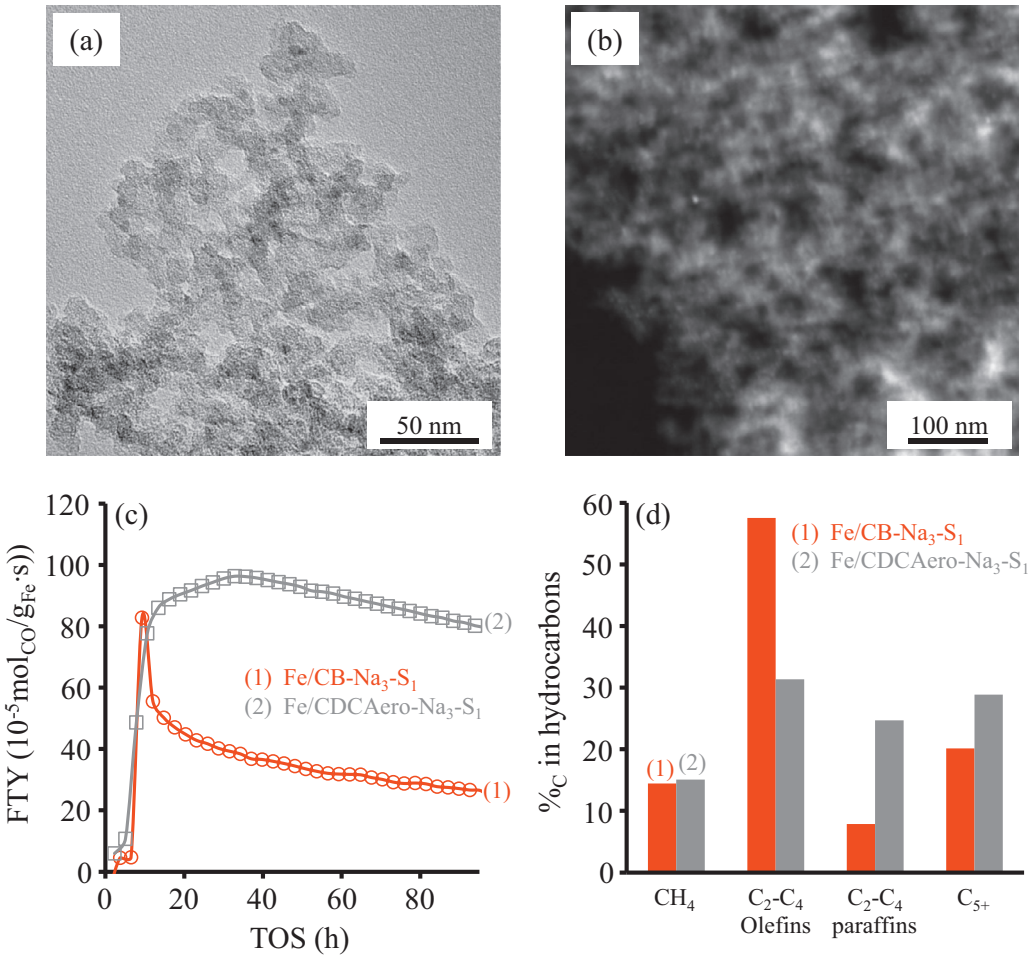

Fig. 5. TEM (a) and HAADF-TEM (b) images of the calcined Fe/CDC–Aero–Na_3–S_1 catalyst as well as FTY over TOS (c) and product selectivity based on the formed hydrocarbons (d) in comparison to the Fe/CB–Na_3–S_1 catalyst under industrially relevant FTO conditions at 10 bar. The selectivities of both catalysts were determined after ~95 h of TOS at CO conversions of ~25% for Fe/CB–Na_3–S_1 and ~75% for Fe/CDC–Aero–Na_3–S_1.

sulfur addition slightly suppresses methane and C_2–C_4 paraffin formation. Under industrially relevant FTO conditions, the iron carbide formation is accelerated for catalysts with higher sodium levels. Iron particle growth during catalyst operation leads to rapid and complete deactivation of the catalysts with 15 or 30 wt% sodium. We refer this to the decrease of available iron carbide surface during particle growth and complete blocking of the active sites with promoters. In general, particle growth occurs independent of the promoter level but seems to be slower with decreasing sulfur content. Despite the comparable particle growth rate as for samples with higher promoter level, catalysts with 3% or 1% sodium maintain significant activity over time on stream because active sites remain available at low promoter contents. For higher sodium contents, the decrease of the iron surface area due to particle growth leads to blocking of the active sites with promoters. Effective suppression of alkane formation by sulfur similarly requires a minimum amount of sodium. For the elevated carbon black support and iron loading, the optimum promoter loadings are 3 wt% sodium and 0.5–1 wt% sulfur with respect to iron. The resulting catalysts combine high catalytic activity and slow deactivation with sufficient suppression of methane formation and high selectivity to C_2–C_4 olefins. A hierarchical CDC aerogel reference support shows that the pore structure of the carbon has significant influence on the distribution of the promoters and hence the optimum concentration depends on iron particle size (iron loading), and support pore structure.

Acknowledgments

We thank Helen de Waard (Utrecht University, Faculty of Geosciences) for the ICP-OES measurements and Tow W. van Deelen (Utrecht University, Group of Inorganic Chemistry and Catalysis) for experimental assistance. We also thank Professor Stefan Kaskel (Technical University Dresden, Inorganic Chemistry) for providing the reference carbon support.

Supplementary materials

Supplementary material associated with this article can be found, in the online version, at doi:10.1016/j.jechem.2016.10.011.

References

[1] H.M. Torres Galvis, K.P. de Jong, ACS Catal. 3 (2013) 2130–2149.
[2] A. Corma, F.V. Melo, L. Sauvanaud, F. Ortega, Catal. Today 107–108 (2005) 699–706.
[3] G. Cai, Z. Liu, R. Shi, C. He, L. Yang, C. Sun, Y. Chang, Appl. Cat. A Gen. 125 (1995) 29–38.
[4] U. Olsbye, S. Svelle, M. Bjørgen, P. Beato, T.V.W. Janssens, F. Joensen, S. Bordiga, K.P. Lillerud, Angew. Chem. Int. Ed. 51 (2012) 5810–5831.
[5] F. Jiao, J. Li, X. Pan, J. Xiao, H. Li, H. Ma, M. Wei, Y. Pan, Z. Zhou, M. Li, S. Miao, J. Li, Y. Zhu, D. Xiao, T. He, J. Yang, F. Qi, Q. Fu, X. Bao, Science 351 (2016) 1065–1068.
[6] K. Cheng, B. Gu, X. Liu, J. Kang, Q. Zhang, Y. Wang, Angew. Chem. Int. Ed. 55 (2016) 4725–4728.
[7] K. Cheng, V.V. Ordomsky, B. Legras, M. Virginie, S. Paul, Y. Wang, A.Y. Khodakov, Appl. Catal. A Gen. 502 (2015) 204–214.

[8] V.R.R. Pendyala, U.M. Graham, G. Jacobs, H.H. Hamdeh, B.H. Davis, ChemCatChem 6 (2014) 1952–1960.
[9] V.P. Santos, T.A. Wezendonk, J.J.D. Jaén, A.I. Dugulan, M.A. Nasalevich, H.U. Islam, A. Chojecki, S. Sartipi, X. Sun, A.A. Hakeem, A.C.J. Koeken, M. Ruitenbeek, T. Davidian, G.R. Meima, G. Sankar, F. Kapteijn, M. Makkee, J. Gascon, Nat. Commun. 6 (2015) 6451.
[10] T.H. Pham, X. Duan, G. Qian, X. Zhou, D. Chen, J. Phys. Chem. C 118 (2014) 10170–10176.
[11] C. López, A. Corma, ChemCatChem 4 (2012) 751–752.
[12] H.M. Torres Galvis, J.H. Bitter, C.B. Khare, M. Ruitenbeek, A.I. Dugulan, K.P. de Jong, Science 335 (2012) 835–838.
[13] T.A. Wezendonk, V.P. Santos, M.A. Nasalevich, Q.S.E. Warringa, A.I. Dugulan, A. Chojecki, A.C.J. Koeken, M. Ruitenbeek, G. Meima, H.-U. Islam, G. Sankar, M. Makkee, F. Kapteijn, J. Gascon, ACS Catal. 6 (2016) 3236–3247.
[14] B. An, K. Cheng, C. Wang, Y. Wang, W. Lin, ACS Catal. 6 (2016) 3610–3618.
[15] J. Tu, M. Ding, Q. Zhang, Y. Zhang, C. Wang, T. Wang, L. Ma, X. Li, ChemCatChem 7 (2015) 2323–2327.
[16] B. Sun, K. Xu, L. Nguyen, M. Qiao, F.F. Tao, ChemCatChem 4 (2012) 1498–1511.
[17] M. Casavola, J. Hermannsdörfer, N. de Jonge, A.I. Dugulan, K.P. de Jong, Adv. Funct. Mater. 25 (2015) 5309–5319.
[18] J. Xie, H.M. Torres Galvis, A.C.J. Koeken, A. Kirilin, A.I. Dugulan, M. Ruitenbeek, K.P. de Jong, ACS Catal. 6 (2016) 4017–4024.
[19] H.M. Torres Galvis, J.H. Bitter, T. Davidian, M. Ruitenbeek, A.I. Dugulan, K.P. de Jong, J. Am. Chem. Soc. 134 (2012) 16207–16215.
[20] W. Chen, Z. Fan, X. Pan, X. Bao, J. Am. Chem. Soc. 130 (2008) 9414–9419.
[21] X. Chen, D. Deng, X. Pan, X. Bao, Chin. J. Catal. 36 (2015) 1631–1637.
[22] K. Cheng, M. Virginie, V.V. Ordomsky, C. Cordier, P.A. Chernavskii, M.I. Ivantsov, S. Paul, Y. Wang, A.Y. Khodakov, J. Catal. 328 (2015) 139–150.
[23] L.M. Chew, W. Xia, H. Düdder, P. Weide, H. Ruland, M. Muhler, Catal. Today 270 (2016) 85–92.
[24] X. Chen, D. Deng, X. Pan, Y. Hu, X. Bao, Chem. Commun. 51 (2015) 217–220.
[25] J. Lu, L. Yang, B. Xu, Q. Wu, D. Zhang, S. Yuan, Y. Zhai, X. Wang, Y. Fan, Z. Hu, ACS Catal. 4 (2014) 613–621.
[26] X. Duan, D. Wang, G. Qian, J.C. Walmsley, A. Holmen, D. Chen, X. Zhou, J. Energy Chem. 25 (2016) 311–317.
[27] P. Zhai, C. Xu, R. Gao, X. Liu, M. Li, W. Li, X. Fu, C. Jia, J. Xie, M. Zhao, X. Wang, Y.-W. Li, Q. Zhang, X.-D. Wen, D. Ma, Angew. Chem. Int. Ed. 55 (2016) 9902–9907.
[28] J. Xie, J. Yang, A.I. Dugulan, A. Holmen, D. Chen, K.P. de Jong, M.J. Louwerse, ACS Catal. 6 (2016) 3147–3157.
[29] H.M. Torres Galvis, A.C.J. Koeken, J.H. Bitter, T. Davidian, M. Ruitenbeek, A.I. Dugulan, K.P. de Jong, J. Catal. 303 (2013) 22–30.
[30] H. Schulz, Catal. Today 228 (2014) 113–122.
[31] G.F. Botes, T.C. Bromfield, R.L.J. Coetzer, R. Crous, P. Gibson, A.C. Ferreira, Catal. Today 275 (2016) 40–48.
[32] X. Zhou, J. Ji, D. Wang, X. Duan, G. Qian, D. Chen, X. Zhou, Chem. Commun. 51 (2015) 8853–8856.
[33] J.D. Xu, Z.Y. Chang, K.T. Zhu, X.F. Weng, W.Z. Weng, Y.P. Zheng, C.J. Huang, H.L. Wan, Appl. Catal. A Gen. 514 (2016) 103–113.
[34] M. Oschatz, W.S. Lamme, J. Xie, A.I. Dugulan, K.P. de Jong, ChemCatChem 8 (2016) 2846–2852.
[35] M. Oschatz, W. Nickel, M. Thommes, K.A. Cychosz, M. Leistner, M. Adam, G. Mondin, P. Strubel, L. Borchardt, S. Kaskel, J. Mater. Chem. A 2 (2014) 18472–18479.